Journal of Korean Powder Metallurgy Institute
Vol. 10, No. 6, 2003

P M 리 뷰

Studies on Microstructural Phenomena Caused by Atomic Diffusion in Sintered Materials

Koji Hayashi
Institute of Industrial Science, The University of Tokyo
(Received 5 November 2003 ; Accepted form 9 November 2003)

Abstract During the sintering of powder materias, many these are microstructural phenomena are caused by atomic diffusion. (1) neck formation and compact densification, (2) grain growth, i.e., growth of matrix grains and dispersed grains, (3) alloying or generation of compound, (4) generations of peculiar and hard layers near sintered compact surface, etc. The studies of the present author and co-workers on these phenomena which were carried out during 40 years are briefly introduced.

1. Sintering

1.1. Preparation of Porous Sintered Compact with Easily Oxidizable Elements[1)]

Chromel/alumel porous sintered compact joint with about 60% of theoretical density is expected as a high temperature thermoelectric transducer. This is because such porous joint enables a sharp temperature gradient between hot and cold junctions by flowing a mixture of inflammable gas and air through the continuous pores and by burning the mixture at the outlet. The preparation of their sintered compact is rather difficult, because chromel and alumel alloys contain easily oxidizable elements, i.e., Cr and Al, respectively.

However, we could prepare their porous sintered compacts and their joint with high ductility or bendability by controlling the sintering atmosphere based on thermodynamics, especially by minimizing the leak velocity in the sintering furnace so that the neck can be formed without oxidation. The SEM micrographs of the cross section of the joint, are shown in Fig. 1.

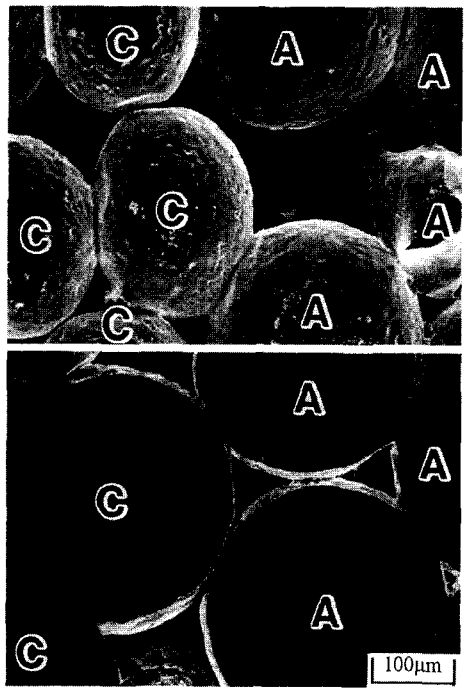

Fig. 1. SEM microstructure of the surface (a) and cross-section (b) of alumel/cromel porous sintered compact join for thermoelectic transducer.

1.2. Proposal of Hypothesis "Equilibrium Gas Pressure in Closed Pores" for Incomplete Sintering Densification of MIM Compact[2,3)]

The relative density of green compact of fine metal powder with mean particle size 5~15 μm for MIM (Metal Injection Molding) is abut 60%, and the compact easily densifies up to about 95% of theoretical density by sintering. The relative density, however, generally saturates near 95~98%. Such incomplete densification could not be explained by well-known theory "Separation of grain boundaries from closed pores": the diffusion distance of vacancies emitted from closed pores to the grain boundaries acting vacancy sinks

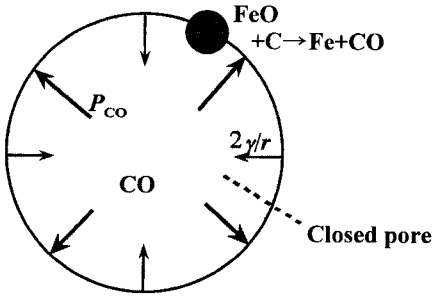

$P_{CO} \geqq 2\gamma/r$: non-shrinkage or expansion

$P_{CO} \leqq 2\gamma/r$: shrinkage

$$P_{CO}=a_{FeO}a_C/a_{Fe}\exp(-\Delta G^0/RT)$$
$$=a_C\exp(-\Delta G^0/RT)$$

Fig. 2. Schematic drawing of the hypothesis "Equilibrium gas pressure in closed pores" for explaining the incomplete sintering densification of MIM compact, i.e., the non-shrinkage or expansion of closed pores.

becomes longer and thus the shrinkage rate of closed pore becomes slower. Then, we proposed the following new hypothesis "Equilibrium gas pressure in close pores", which is based on thermodynamics.

(i) Gases such as CO or H_2O generated by the reduction reaction of residual oxide with impurity carbon of sintered compact or sintering atmosphere H_2 are entrapped in closed pores.

(ii) If the equilibrium pressure of such entrapped gases is higher than the surface stress of closed pore ($\sigma=2\gamma/r$, where γ : surface tension, r: radius of closed pore), i.e., the driving force for densification, the densification of the compact becomes incomplete, and vice versa, as schematically shown in Fig. 2 in the case of CO gas in Fe compact containing FeO and C. The equilibrium (P_{CO}) of CO gas entrapped in closed pore is expressed by the following equation.

$$P_{CO}=a_{FeO}a_c/a_{Fe}\exp(-\Delta G^0/RT)$$

Where, a is activity (a_{FeO}, a_{Fe}=1), G^0, is Gibbs standard free energy change in the reduction reaction of FeO+C→Fe+CO, R is gas constant, and T is sintering temperature. In the case of Cu sintered in H_2 atmosphere, H_2O gas pressure is important.

Our hypothesis was supported by the experimentall result that the addition of metals forming stable oxide, i.e., metals reducing P_{CO} or P_{H_2O} causes the complete densification, and vice versa

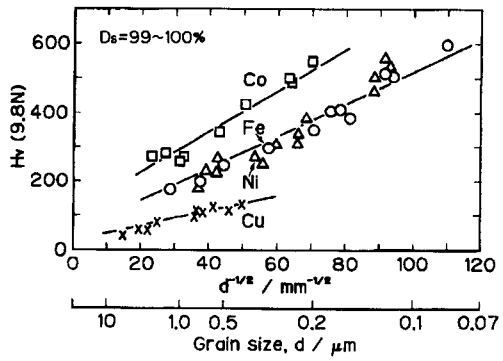

Fig. 3. Hall-Petch relation between hardness (Hv) and the inverse of square root of grain size is observed also in the grain size of 2.0~0.09 μm. The metal were prepared by hot-pressing of ultra fine powder with mean particle size of 0.02~0.05 μm.

2. Grain Growth

2.1. Preparation of Fine Grained Metals and Alloys with One Phase from Ultra-Fine Powder[4,5]

By hot pressing of ultra-fine Fe, Co, Ni and Cu metal powders with mean particle size of 0.02~0.05 μm, we prepared fine grained metals and alloys with mean grain size of 2.0~0.09 μm. Hall-Petch relation between hardness and the inverse of square root of grain size was observed also in these fine grain size range as shown in Fig. 3 in the same way as in the coarse grain size range above 10. The Vickers hardness (Hv) of Fe metal and Fe-50at%Co alloy were extremely high irrespective of the absence of dispersed particles, i.e., about 600 at 0.09 μm and 900 at 0.12 μm, respectively. These values suggest that the yield strength (~1/3 of Hv) of these metal or alloy can reach about 2 GPa and 3 GPa, respectively.

2.2. Numerical Calculation of WC Grain Growth in VC-Doped WC-Co Fine Grained Hardmetal[6]

The mean grain size of WC grains in commercial fine-grained WC-Co hardmetal are set above about 0.5 μm, although the more finer WC powders are commercially available. This seemed to be because the grain growth becomes considerable, when the more finer WC powder is used. The candidates for the cause for such considerable grain growth were (1) large grain size distribution, (2) non-uniform distribution of grain growth inhibitor such as VC and Cr_3C_2, ets. Then, we derived an equation for WC grain growth in two-grain size alloy model and in multi-grain size

alloy model, where the growth mechanism is Ostwald ripening and the rate-determining step of the growth is the precipitation process.

For example, the large WC grain size ($d_{L,\ t+\Delta t}$) in two-grain size alloy model is expressed at sintering time of $t+\Delta t$ by the following differential equation.

$$d_{L,t+\Delta t} = d_{L,t} + 4(2\sigma\kappa C_0 V_m^2/\nu RT)(1/d_{F0} - 1/d_{L,t})\Delta t$$

Where, Δt is the increment of sintering time, σ is the interfacial energy between WC and Co, κ is the interfacial reaction rate constant at WC/Co, C_0 is the equilibrium solubility (molar concentration) of WC in Co liquid phase, V_m is the molar volume of WC, ν is a correction factor which depends on shape and contiguity of WC grains, R is gas constant and d_{F0} is the size of small grain at sintering time of zero.

The result of calculation by using the experimental value of the term of $2\sigma\kappa C_0 V_m^2/\nu RT$ which corresponds to the slope of $d_m^2 - t$ curve(d_m : WC mean grain size) and which was considered not to be affected by non-uniform distribution of grain growth inhibitor showed the following: abnormal or considerable grain growth occurs even under the condition that the large grain size is only twice of small grain size, when the mean particle size of starting WC powder becomes below about 0.2 μm, as schematically shown in Fig. 4. The result of multi-grain size alloy model as well as that of two-grain size alloy model shown in Fig. 4 suggested that the abnormal or considerable grain growth below 0.2 is not due to the large grain size distribution of WC powder, but almost naturally occuring as far as the present preparation method is used.

3. Alloying or Generation of Compound

3.1. Proposal of "Solution/Reaction-Precipitation Mechanism" for Generation of TiC-core/(Ti,Mo) C-rim Structure in TiC-Mo_2C-Ni Cermet[7]

The carbide grains in TiC-Mo_2C-Ni cermet which is prepared from the mixed powder of TiC, Mo_2C and Ni show TiC-core/(Ti,Mo)C-rim structure, although the equilibrium carbide phase is only (Ti,Mo)C. The example of SEM microstructure of core/rim structure is shown in Fig. 5. The previous papers reported that

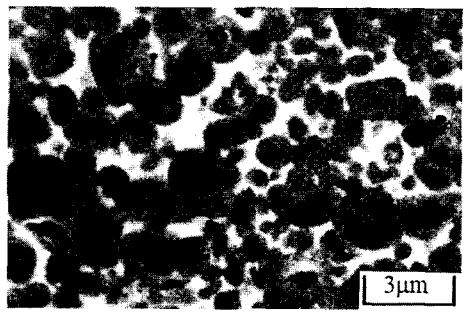

Fig. 5. SEM micrograph of TiC-core/(Ti,Mo)-rim structure in TiC-Mo_2C-Ni cermet.

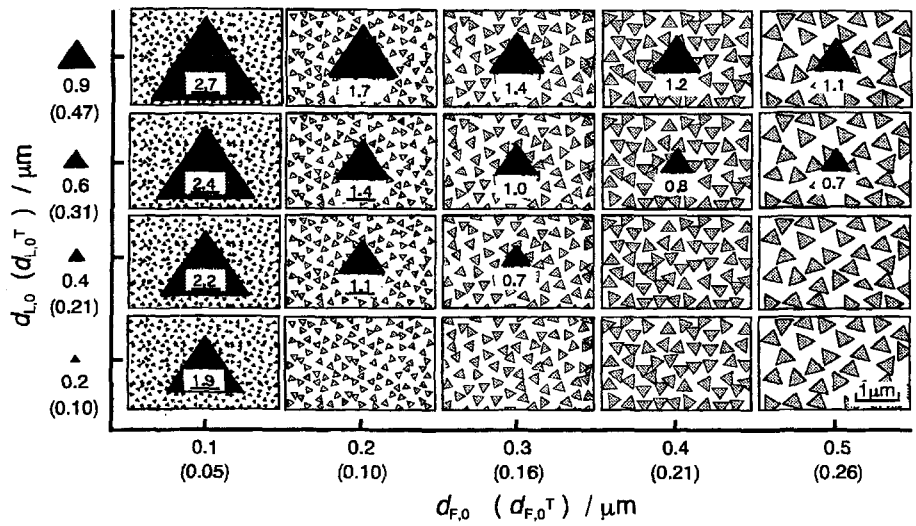

Fig. 4. Schematic drawing of the calculation result of large grain size as a function of the initial large and small grain sizes ($d_{L,0}$,$d_{s,0}$) in two grain size alloy model.

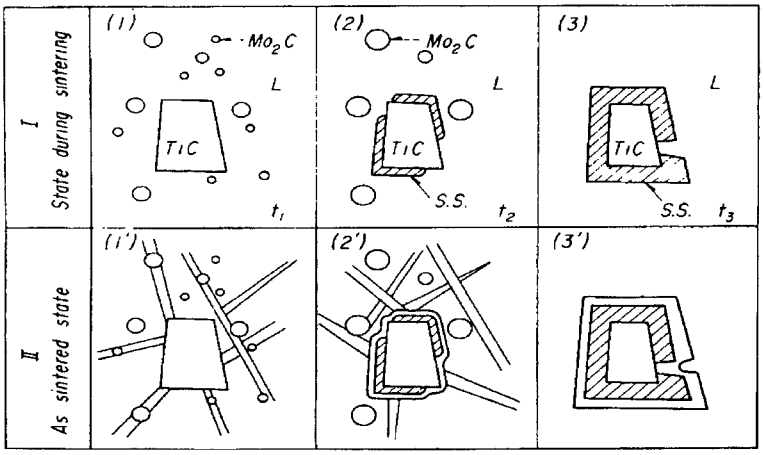

Fig. 6. Schematic drawing of "Solution/reaction- precipitation mechanism" for TiC-core/(Ti,Mo)-rim structure in TiC-Mo_2C-Ni cermet.

such structure is supposed to be generated by solid diffusion of Mo and C atoms into the periphery of TiC grain. We clarified that the structure is generated by the following "solution/reaction-precipitation mechanism". as schematically shown in Fig. 6.

(i) Smaller TiC grains and Mo_2C grains dissolve into Ni liquid phase.{I-(1) in Fig. 6}

(ii) Ti, Mo and C solutes in Ni liquid phase diffuse toward near larger TiC grains and reaction-precipitate on the larger TiC grains in the form of (Ti,Mo)C phase, resulting in the generation of rim.{I-(2) in Fig. 6}

(iii) The thickness of the rim increases by Ostwald ripening together with the disappearance of smaller grains and without the shrinkage of residual TiC-core. {I-(3) in Fig. 6}

(iv) The thickness of the rim further increases by a small amount by the precipitation of the solute during the cooling stage of sintering cycle. {II-(1) in Fig. 6}

The result of XMA analysis on Mo concentration profile in TiC-core/(Ti,Mo)C-rim structure supported the hypothesis.

3.2. Proposal of New Hypothesis "Exhaustion of Diffusion-Contributable Atomic Vacancies in Core/Rim Structure"[8-10]

$FeSi_2$ is expected as a high temperature thermoelectric material. This $FeSi_2$ is supposed to be generated by a peritectoid reaction of $FeSi+Fe_2Si_5 \rightarrow 3FeSi_2$, etc., in Fe-66.7at%Si alloy according to Fe-Si equilibrium phase diagram. The reaction, however, hardly progresses even by long-time heating at high temperature, resulting in the generation of FeSi-core/$FeSi_2$-rim structure embeded in matrix of Fe_2Si_5 or $FeSi_2$+Si among which $FeSi_2$+Si structure is generated by the decomposition of Fe_2Si_5. This phenomenon has traditionally been explained to be due to the increasing of the rim thickness, i.e., the diffusion distance, accompanying the progress of the peritectoid reaction. In contrast with this traditional explanation, we proposed the following new hypothesis "Exhaustion of diffusion-contributable atomic vacancies in core/rim structure", the schematic diagram of which is shown in Fig. 7.

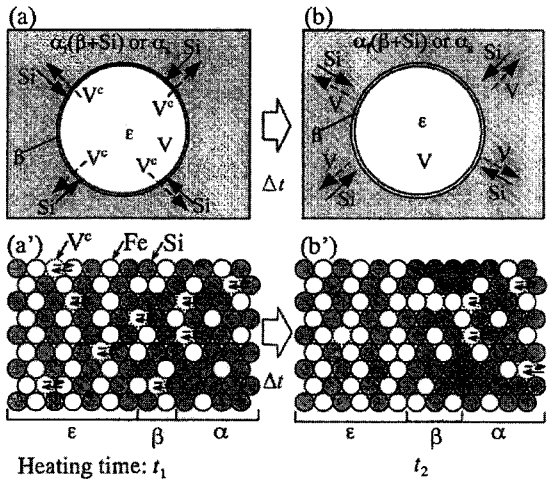

Fig. 7. Schematic drawing of hypothesis "Exhaustion of diffusion-cotributable atomic vacancies in core/rim structure".

(i) For the progressing of the peritectoid reactions, Si atoms in the matrix of Fe_2Si_5 or $FeSi_2$+Si need to

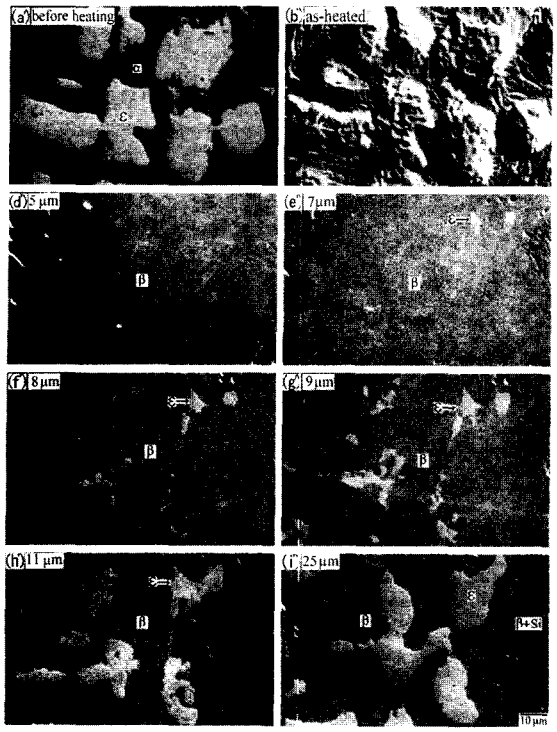

Fig. 8. A proof for the hypothesis shown in Fig. 7. FeSi-cores disappeared near sintered compact surface, differing from those in compact inside, by heating at 1123K for 720 ks.

diffuse to the closed interface of FeSi-core/$FeSi_2$-rim (reaction site) via $FeSi_2$-rim, and at the same time the atomic vacancies in FeSi-core and $FeSi_2$-rim structure should diffuse in counter-wise direction.

(ii) Such mutual counter-wise diffusions strongly suppress the diffusion of atomic vacancies from the matrix to FeSi-core and thus causes the exhaustion of diffusion-contributable atomic vacancies in FeSi-core and $FeSi_2$-rim structure resulting in the extremely slow rate of the peritectoid reaction.

This hypothesis has already been verified by the phenomenon shown in Fig. 8 that the reaction completely finished near the compact surface where atomic vacancies are abundantly supplied from the interface of compact surface/vacuum atmosphere.

This hypothesis can be applied to core/rim structure where the rim is a stoichiometric compound and the diffusion from core to rim and matrix is thermodynamically inhibited like in FeSi-core/$FeSi_2$-rim structure, and not applied to the structure where the rim is not a stoichiometric compound and the mutual diffusion between core and rim is thermodynamically allowed like in TiC-core/(Ti,Mo)C-rim structure in TiC-Mo_2C-Ni cermet.

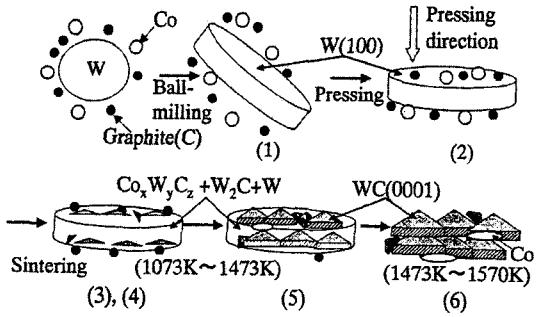

Fig. 9. Schematic drawing for generation process of highly oriented plate-like WC grain in WC-Co base hardmetal prepared from W+C+Co base mixed powder instead of usual WC+Cobase mixed powder. The numbers in the figure are those in the original figure in Ref.11.

3.3. Proposal of Mechanism for Formation of Highly Oriented Plate-Like Triangular Prismatic WC Grains in WC-Co Base Hardmetal Prepared from W+C Mixed Powder Instead of WC Powder[11,12]

WC-Co base hardmetal with highly oriented plate-like triangular prismatic WC grains can be prepared by using W+C mixed powder instead of usual WC powder. The rest of the preparation processes are the same as usual: ball milling, unidirectional die-compaction, pressureless vacuum sintering. The properties such as transverse-rupture strength and fracture toughness at an identical hardness is superior to those of conventional WC-Co base hardmetal.

The mechanism for the formation of such highly oriented plate-like WC grains was clarified to be as follows, as schematically shown in Fig. 9.

(1) Granular W powder particles are flattened by ball-milling to become plate-like.

(2) Such plate-like W particles are highly oriented vertically to the pressing direction by unidirectional powder die-compaction with high compaction ratio.

(3) At temperatures below the Co-W-C liquid appearing temperature in sintering process, $Co_xW_YC_z$ (η-type compound) is mainly generated in plate-like W particles together with W_2C by the reaction among Co, W and C. Thus, the shape of $Co_xW_YC_z$+W_2C+W agglomerate particles are also plate-like.

(4) Then, WC grains are generated in the particle mainly by the reaction of $Co_xW_YC_z$+residual CWC+

Co. The nucleation and/or growth of such WC particles having (0001) crystal plane oriented parallel to the plane of plate-like $Co_XW_YC_Z$+W_2C+W agglomerate particles preferentially occurs, compared with those of WC particles having other crystal planes. This is because the growth rate of $(10\bar{1}0)$ columnar plane is larger than (0001) basal plane and the diffusion distance of C atoms to the columnar plane is of course shorter for WC grains whose basal plane is parallel to the plate-like plane than the others. This leads to a lot of generation of WC grain with (0001) plane vertical to the die-pressing direction.

(5) The orientation of plate-like WC grains in the above solid state is kept during the appearance and solidification of Co-W-C liquid phase, resulting in the sintered alloy with highly oriented plate-like triangular prismatic WC grains.

3.4. Proposal of Atomic Models for Formation Process of New Carbonitride W(C, N)Synthesized by Normal- and High-Pressure Methods[13,14]

The synthesis of new mono-carbonitride of W, i.e., W(C,N) which is thermodynamically not possible by using nitrogen gas at normal pressure, was succeeded by using CH_4+NH_3 mixed gas of normal pressure (normal pressure method)and also by using C powder + nitrogen gas of high pressure (high pressure method). The maximum N contents of W (C,N) obtained by both methods were 7 and 24 at%, repectively. The formation of the mono-carbonitride as well as general compounds generated by these methods have been explained by applying traditional Ostwald's step rule and virtual-pressure concept for normal pressure for normal pressure method, and Le Chatelier's principle for high pressure method, respectively. These explanations are based only on the macroscopic level, which give us no image of atom movement during the reaction.

Then, we newly proposed the following atomic models for the formation process of W(C,N) in both methods.

(i) Nascent N-atoms are generated at low temperature of 973~1073 K in normal pressure and nascent C-atoms are also generated near synthesizing temperature of 1173~1373 K, a part of which is schematically shown is Fig. 10(a). On the other hand in high pressure method, N-clusters are generated above 3.35 MPa near synthesizing temperature of 1173~1373 K, as schematically shown is Fig. 10(b), because

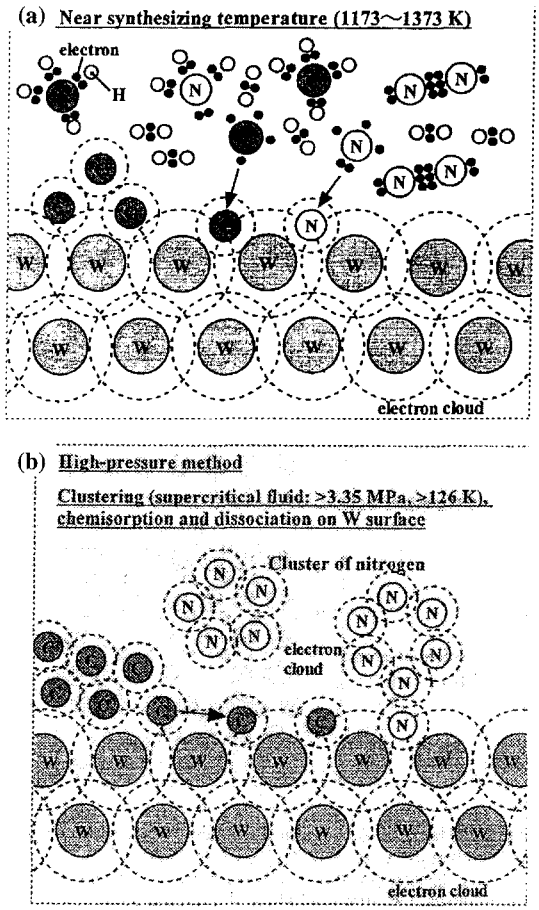

Fig. 10. Schematic drawing of atomic model for reaction process of N atoms with W crystal lattice in normal pressure method (a) and high pressure method (b).

N gas becomes supercritical fluid above pressure and 126 K.

(ii) These nascent N atoms and N clusters chemisorp on the surface of W powder particles together with C atoms, as schematically shown also in those figures, differing from N_2 gas of normal pressure.

(iii) Such chemisorped N atoms and the N atoms of such chemisorped clusters diffuse into W crystal lattice together with C atoms, and then W(C,N) is formed, when the solubility of diffused atoms exceed the equilibrium solubility.

This model is based on the following idea: (1) the atomic bonding energy between two N atoms of N_2 molecule with triple bond ($N \equiv N$) is so high that the N atom is unable to react with W even in the presence of C atoms, differing from nascent N atoms and

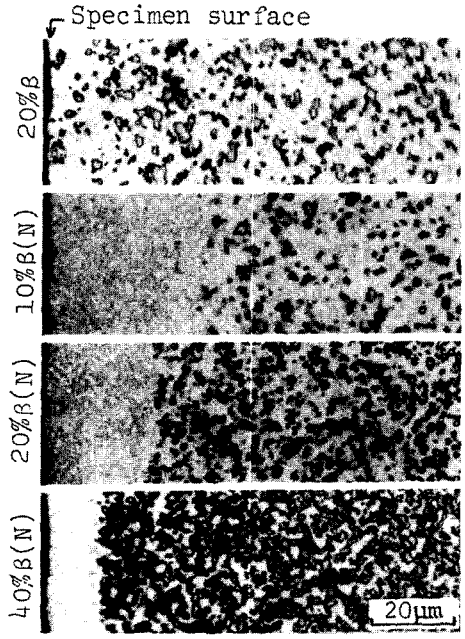

Fig. 11. Optical microstructure of (W,Ti)(C,N)-free layer observed near compact surface of WC-(W,Ti)(C,N)-Co hardmetal.

N atoms in N-cluster, and (2) W(C,N) is thermodynamically stable under the coexistence of nascent N atoms or N-clusters and C atoms.

4. Generation of Peculiar and Hard Layers near Sintered Compact Surface

4.1. Proposal of Mechanism for Generation of (W,Ti)(C,N)-Free Layer near Compact Surface of WC-(W,Ti)(C,N)-Co Hardmetal[15]

WC-(W,Ti)(C,N)-Co vacuum-sintered hardmetal which has (W,Ti)(C,N)-free thin layer, i.e., WC+Co thin layer of thickness of about 10, near the compact surface as shown in Fig. 11, is commercially used as the substrate alloy for CVD coated cutting tools. This is because the layer has high resistance to the propagation of cracks in CVD-coated layer toward the substrate alloy, compared with normal WC+(W,Ti)(C,N) +Co structure. We proposed the following mechanism for the generation which is schematically shown in Fig. 12.

(i) Denitriding occurs from the compact surface at sintering temperature.

(ii) Then, the N content or N+C content in Ni liquid phase near the compact surface decreases, which

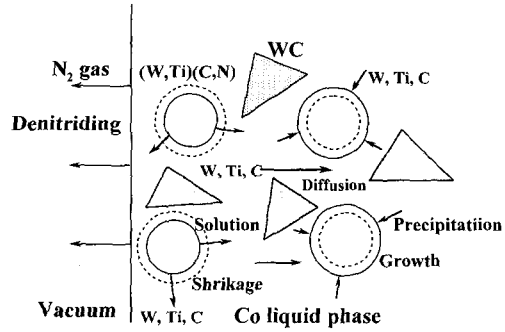

Fig. 12. Schematic drawing of generation process of (W,Ti)(C,N)-free layer shown in Fig. 11.

causes the increase of the equilibrium solubility of (W,Ti)(C,N) phase, i.e., the contents of Ti and Mo, in Ni liquid phase near the compact surface.

(iii) Then, Ti, W and C solutes in Ni liquid phase diffuse from near the compact surface to the compact inside and precipitate on (W,Ti)(C,N) grains in the compact inside.

(iv) The processes from the above (i), (ii) and (iii) repeatedly continues, and thus (W,Ti)(C,N) grains shrink and then disappear near the compact surface, together with the growth of (W,Ti)(C,N) grains in the compact inside.

The rate-determining step of the generation was supposed not to be the denitriding process, but to be W and Ti diffusions toward the compact inside, because the thickness of (W,Ti)(C,N)-free layer near the edge of compact is smaller than that near usual flat surface.

This mechanism clearly explain the experimental results on the influences of factors such as the contents of N, C and (W,Ti)(C,N) and the sintering atmosphere on the thickness of (W,Ti)(C,N)-free layer.

4.2. Formation of Hard Layer on Compact Surface of WC-(W,Ti)C-Co Hardmetal by Diffusion Process[16]

Based on the study shown in the above section (4.1), it was suggested that (W,Ti)(C,N)-or (W,Ti)C-rich layer is formed by heating WC-(W,Ti)C-Co alloy in N_2 or CH_4 atmosphere, because the equilibrium solubility of Ti in Co liquid phase decreases near the compact surface by nitriding or carburizing. Namely, (W,Ti)C grains in the compact inside dissolve in Co liquid phase, then thier solutes diffuse to the compact surface and precipitate on (W,Ti)C grain near the com-

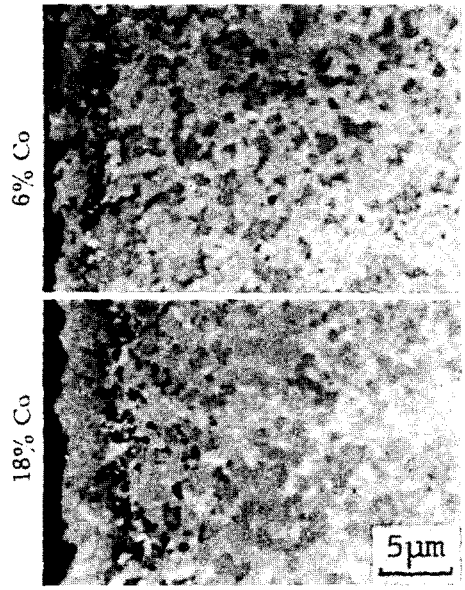

Fig. 13. Optical microstructure of (W,Ti)C-rich layer generated by heating WC-(W,Ti)C-Co hardmetal in CH_4 atmosphere.

pact surface together with N or C atoms, resulting in the formation of (W,Ti)(C,N)-or(W,Ti)C-rich layer. The result was as expected, as shown in Fig. 13 for CH_4 atmosphere

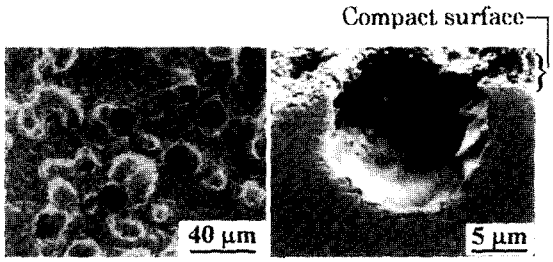

Fig. 14. Open pore generated near compact surface of vacuum sintered Ti(C,N)-Mo_2C-Ni cermet. (a) compact surface and (b) the cross-section.

4.3. Proposal of Mechanism for Generation of Open Pores on Sintered Surface of Ti(C,N)-Mo_2C-Ni Cermet[17]

Open pores, i.e., pores connecting to the compact surface, whose diameter are in the range of 10–100 μm, tend to be generated in Ti(C,N) base cermet. An example is shown in Fig. 14. It was found that the generation occurs, when the atmosphere in the temperature-keeping stage during sintering is vacuum (7 Pa), irrespective of the kind of atmospheres (vacuum and nitrogen of 0.13 Pa) in the temperature-raising and cooling stage, and vice versa. The mechanism, which is schematically shown in Fig. 15, was supposed as follows, mainly based on the various experimental results.

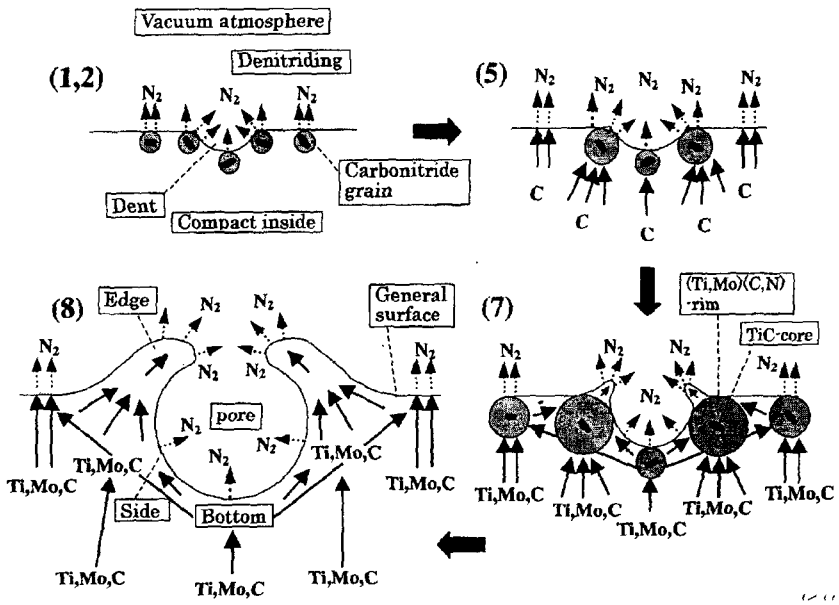

Fig. 15. Schematic drawing of generation process of open pore shown in Fig. 14. The number in the figure are those in the original figure in Ref. 17.

(i) The generation and the growth of open pores is caused by denitriding from the compact surface to the sintering atmosphere. The denitriding occurs more rapidly from the compact surface having larger ratio of surface-area/volume.{(1),(2) in Fig. 15}

(ii) Then, nitrogen concentration gradient occurs among the edge, side and bottom of dents or cracks and the general compact surface.

(iii) Such N concentration gradient causes the transports of C atoms in the compact inside toward the above each place of the compact surface and then caused the transports of Ti and Mo atoms mainly from the side and bottom of the dent or cracks to the edge. Such transports of Ti and Mo atom results in both the deepening of the bottom and side and the protruding of the edge, which leads to the generation and growth of open pores.{(7),(8) in Fig. 15}

The methods for inhibiting the generation of open pores were also proposed.

Beside the above phenomena, high temperature fracture and creep rupture of WC-Co base hardmetal[18,19] and TiC base cermet[20-22] are also caused by atomic diffusion in the binder phase under stress. The widening of the normal phase region, i.e., the region free from free carbon and $Co_3W_3C(\eta)$ phases, of WC-Co hardmetal by the addition of TiC or (W,Ti)C is due to the fact that C atoms in Co binder phase diffuse into non-stoichiometric (W,Ti)C phase or vice versa, depending on the carbon content of hardmetal, so that the chemical potentials of the binder and (W,Ti)C phases are balanced with each other[23,24]. The phenomenon that the sintering densification of $BaTiO_3$ PTCR (Positive temperature coefficient of resistivity) thermistor is strongly suppressed by the addition of metallic Ti powder is due to the diffusing-out of O atoms in $BaTiO_3$ crystal lattice, i,e., the generation of large amount of 0^{2-} ion vacancies in $BaTiO_3$ crystal lattice[25].

References

1. Won-Seung Cho, Takehiko Miyazaki, Yoshihiko Doi and Koji Hayashi : Mat. Trans. JIM, **60** (1996) 311-317 (in Japanese).
2. Koji Hayashi and Tai-Whan Lim : Mat. Trans. JIM, **32** (1991) 383-388.
3. Hirotsugu Itoh and Koji Hayashi : Proc. of JSPM Spring Meeting, (1992) 196 (in Japanese).
4. Koji Hayashi and Hiroshi Kihara : Fundamentals of Diffusion Bonding, Studies in Physical and Theoretical Chemistry48, ed. By Yoichi Ishida, Elsevier, (1987) 501-510.
5. Koji Hayashi and Hiroyuki Etoh : Mat. Trans. JIM, **30** (1989) 925-931.
6. Naoki Matsuoka and Koji Hayashi : J. Japan Soc. PM, **47** (2000) 1318-1327.
7. Hisashi Suzuki, Koji Hayashi and Osamu Terada : J. Japan Inst. Met. **35** (1971) 936-942 (in Japanese).
8. Masanori Tajima and Koji Hayashi : J. Japan Soc. PM, **46** (1999) 757-766.
9. Nobuto Taniguchi and Koji Hayashi : J. Japan Soc. PM, **48** (2001) 501-511.
10. Yutaka Yanaba and Koji Hayashi : J. Japan Soc. PM **50** (2003) to be contributed.
11. Satoshi Kinoshita, Takeshi Saito, Masaki Kobayashi and Koji Hayashi : J. Japan Soc. PM, **48** (2001) 51-60.
12. Kozo Kitamura, Masaki Kobayashi and Koji Hayashi : J. Japan Soc. PM, **48** (2001) 621-627.
13. Nobuaki Asada, Yoshiharu Yamamoto, Tadashi Igarashi, Yoshihiko Doi and Koji Hayashi : J. Japan Soc. PM, **47** (2000) 496-501.
14. Kazuhiko Tanaka, Nobuaki Asada and Koji Hayashi : J. Japan Soc. PM, **50** (2003) 534-544.
15. Hisashi Suzuki, Koji Hayashi and Yasuro Taniguchi : Trans. JIM **22** (1981) 758-764.
16. Koji Hayashi, Naomi Namiki, Yodhio Takashima and Koji Hayashi : J. Japan Soc. PM, **29** (1982) 159-163 (In Japanese).
17. Nobuo Hojo, Satoshi Kinoshita, Yasuro Taniguchi and Koji Hayashi : J. Japan Soc. PM, **50** (2003) 385-395.
18. Hisashi Suzuki, Koji Hayashi and Yasuro Taniguchi : Planseeberichte fuer Pulvermet., **25** (1977) 23-31.
19. Hisashi Suzuki, Koji Hayashi and Wan Jae Lee : Planseeberichte fuer Pulvermet., **25** (1977) 186-194.
20. Hisashi Suzuki, Koji Hayashi and Tsutomu Yamamoto : J. Japan Soc. PM, **26** (1979) 22-26 (in Japanese).
21. Hisashi Suzuki, Koji Hayashi and Yutaka Kubo : J. Japan Soc. PM, **27** (1980) 266-272 (in Japanese).
22. Hisashi Suzuki, Koji Hayashi Hideaki Matsubara and Kei Tokumoto : J. Japan Soc. PM, **30** (1983) 106-111 (in Japanese).
23. Hisashi Suzuki and Koji Hayashi : Trans. JIM, **7** (1966) 199-203.
24. Hisashi Suzuki, Takaharu Yamamoto and Koji Hayashi : J. Japan Soc. PM, **13** (1966) 304-309.
25. Jun-Gyu Kim, Won-Seung Cho and Koji Hayashi : J. Japan Soc. PM, **47** (2000) 951-957.